Chemical Physics Letters 804 (2022) 139867

Contents lists available at ScienceDirect

Chemical Physics Letters

journal homepage: www.elsevier.com/locate/cplett

Research paper

Understanding the Stokes shift and nonlinear optical behavior of 1-nitro-2-phenylethane: A sequential Monte Carlo/Quantum Mechanics discussion

Franco F. Almeida [a], Lucas Modesto-Costa [a,b], Antonio R. da Cunha [c,d], Darlisson A. Santos [e,f], Tarciso Andrade-Filho [g], Rodrigo Gester [g,*]

[a] Programa de Pós-Graduação em Química, Universidade Federal do Sul e Sudeste do Pará, Marabá-PA, 68507-590, Brazil
[b] Departamento de Física, Universidade Federal Rural do Rio de Janeiro, Seropédica-RJ, 23890-000, Brazil
[c] Universidade Federal do Maranhão, UFMA, Campus Balsas, CEP 65800-000, Maranhão, Brazil
[d] Instituto de Física, Universidade de São Paulo, Rua do Matão 1371, São Paulo, SP 05588-090, Brazil
[e] Faculdade de Química, Universidade Federal do Sul e Sudeste do Pará, Marabá-PA, 68507-590, Brazil
[f] Departamento de Química Fundamental, Universidade Federal de Pernambuco, Recife, 50740-560, Pernambuco, Brazil
[g] Faculdade de Física, Universidade Federal do Sul e Sudeste do Pará, Marabá-PA, 68507-590, Brazil

HIGHLIGHTS

- A great Stokes shift (ca. 70 nm) is reported for a natural drug.
- The solvent effects are available for linear and nonlinear optical properties.
- Improved hyperpolarizabilities in comparison to other standard NLO materials.

GRAPHICAL ABSTRACT

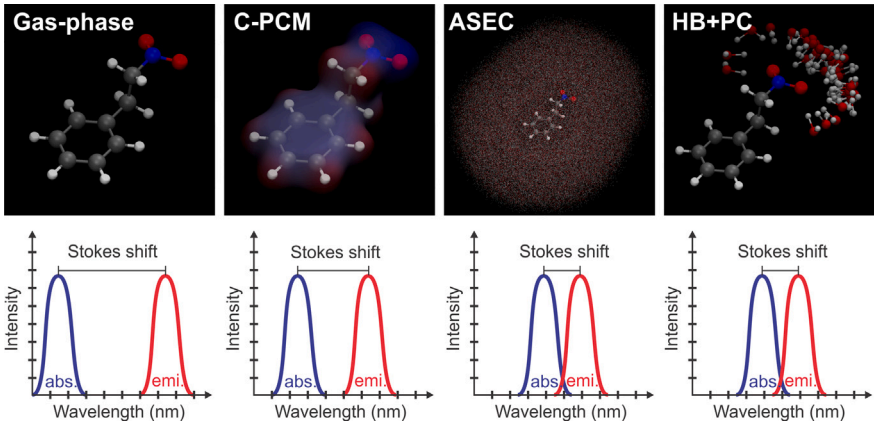

ARTICLE INFO

Keywords:
Stokes shift
Nonlinear optics
DFT methods
Solvent effects
Monte Carlo simulations

ABSTRACT

The linear and nonlinear optical (NLO) properties of 1-nitro-2-phenylethane were studied with Density Functional Theory, and the solvent effect was included with a sequential Monte Carlo/Quantum Mechanics procedure. The analysis shows that the first and second hyperpolarizabilities are respectively twice and thirty-five times larger than those reported for urea, which is a standard NLO material. The results also indicate that the lowest $n-\pi^*$ excitation suffers a pronounced Stokes shift (ca. 70 nm) which is mildly affected by the solvent. Moreover, the title compound presents a low refractive index (1.46 – 1.80). Thus, the results signalize optoelectronic usages in solar cells or biological probes.

* Corresponding author.
E-mail addresses: darlisson@unifesspa.edu.br (D.A. Santos), gester@unifesspa.edu.br (R. Gester).

https://doi.org/10.1016/j.cplett.2022.139867
Received 26 January 2022; Received in revised form 6 July 2022; Accepted 7 July 2022
Available online 15 July 2022

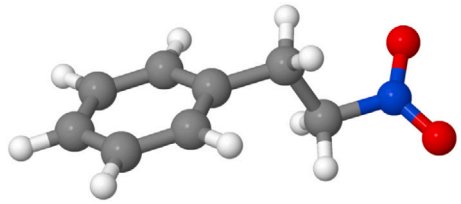

Fig. 1. The 1-nitro-2-phenylethane (NPE) molecule obtained from the *Aniba canelilla* extraction.

1. Introduction

The 1-nitro-2-phenylethane (NPE, see Fig. 1) molecule is the active principle extracted from *Aniba canelilla*, a endemic plant found in the Amazon biome. Along the years, this natural compound has been used against several human diseases like antinociceptive [1], antimicrobial [2], and the recently discovered use as an antifungal [3] drug, but perhaps, the most relevant NPE utilization would be its use in cardiovascular [4] and vasorelaxant [5] therapies. However, although the NPE pharmacological use is well established, many of its chemical–physical properties remain obscured.

The Stokes shift is one of the properties mentioned above. The difference between the maximum of emission and absorption spectra ($\Delta\lambda = \lambda^{em} - \lambda^{abs}$) is called Stokes shift and has great importance for technological applications. For instance, chromophores with pronounced Stokes shift ($\Delta\lambda > 30$ nm) are helpful to build sensors and biological probes to be used as markers in human cancer cells [6,7]. Moreover, although $n - \pi^*$ lines are less intense than strong $\pi - \pi^*$ transitions, these states demand less energy. Due to such properties, the behavior of $n - \pi^*$ transitions is highlighted [8–11].

The nonlinear optical (NLO) behavior of organic chromophores also is the focus of great attention in materials science. This is because, compared to traditional inorganic chromophores, organic molecules have high rupture limits when exposed to a high-power laser, in addition to facilitating the miniaturization of optoelectronic circuits [12].

For the first time, a careful analysis was performed on the linear and nonlinear optical response of the NPE molecule, paying attention to the solute polarization due to solvent and specific solute–solvent interactions. To include the polarization effect we used the sequential Monte Carlo/Quantum Mechanics (s-MC/QM) [10,11], where the classical Monte Carlo simulations are used to generate the liquid configurations for subsequent treatment with Density Functional Theory (DFT) [13,14]. With such formalism, in addition to a discussion on the liquid structure surrounding the solute molecule, we discuss how the solvent impacts linear properties like the dipole moment (μ), dipole polarizability (α), and even the refractive index (n). Moreover, under static and frequency-dependent regimes, we also investigate the impacts of the environment on the first (β) and second (γ) hyperpolarizabilities, which are responsible for the second and third harmonic generation processes [15].

The results reveal that the lowest-lying $n - \pi^*$ excitation the NPE chromophore presents a pronounced Stokes shift in an aqueous solvent, which motivates its use in the designing of solar cells and biological sensors. In addition, the system presents a lower refractive index. Finally, the NPE molecule shows first and second hyperpolarizability higher than urea, which is a standard NLO material. The results suggest that NPE derivatives can be useful for a series of NLO devices.

2. Theoretical details

Under a gaseous environment, the molecular geometry of the NPE was obtained with Density Functional Theory (DFT) using CAM-B3LYP [16] functional and 6-311++G(*d,p*) [17,18] basis set. Both the functional and the base set are well established in the quantum chemistry. The posterior analysis of the Infrared (IR) spectra attested only positive vibrational frequencies, which indicate that the molecular geometry is at a global minimum of energy. The same level was used in the excited state calculation, with the time dependent DFT (TD-DFT).

Concerning the solvent effects, a sequential Monte Carlo/Quantum Mechanics (s-MC/QM) procedure [10,11] was used to account for such properties. In such a protocol, liquid structures are generated and sampled by classical simulations for subsequent treatment with quantum mechanics. Thus, classical simulations have been performed in the *NpT*, with one solute surrounded by 1000 water molecules at $p = 1.0$ atm, and $T = 298.15$ K.

The solute geometry used during the MC simulations was obtained considering a previous polarization due to solvent using the conductor-like polarizable continuum model (C-PCM) [19,20]. Concerning the intermolecular interactions were mediated by the standard Lennard-Jones (LJ) plus the Coulomb potential. While the water parameters were totally represented for the TIP3P potential [21], for the solute molecule, only the LJ parameters were obtained from the all-atom optimized potentials for liquid simulations (OPLS-AA) force field [22]. However, the initial solute charges were extracted in the C-PCM environment, performing the CHELPG fitting of the quantum potential [23] at the CAM-B3LYP/6-311++G(*d,p*) level of quantum mechanics.

The classical simulations were portioned in two stage. In the first one, a thermalization, 7×10^9 MC steps were carried out to reach the thermodynamic equilibrium. Thus, more 9×10^{10} MC steps were performed to obtain liquid structures sampled for subsequent treatment with quantum mechanics. The MC step is the application of the Metropolis MC algorithm to each solvent molecule. The large number of MC steps are necessary to obtain 100 uncorrelated configurations, using as a parameter the maximum value of 15% of autocorrelation between the configurations. The maximum value of step size for the change in molecule position is self-adjusted to maintain the acceptance rate around 50%. The QM calculations were performed considering the following solvent models:

- **C-PCM**: The solvent is modeled as a Conducting version of the Polarizable-Continuum Model [19,20], which is accepted as the most appropriate for NLO calculations between the continuum model family [24].
- **ASEC**: The solvent is represented as an Electrostatic Configuration [25] superposing 100 MC structures composed by one explicit solute molecule surrounded by the 300 nearest water molecules represented by its normalized point charges. This explicit representation of the solvent has been used with success to describe diverse NLO properties [26,27].
- **HB+PC**: This model averages over 100 MC configurations composed by solute–solvent hydrogen-bonded structure embedded in the electrostatic field of the remaining 300 water molecules represented as point charges, and accounts for specific solute–solvent interactions like Keeson, Debye, and London forces present in the hydrogen bonds, as well as the long-range electrostatic effects coming from the bulk molecules. Consequently, this approach is more precise than pure electrostatic models [28,29].

Concerning the NLO properties, these effects arise when the light interacts with the matter. In such a case, the energy of the system can be expanded in Taylor series like

$$E(F) = E(0) - \mu_i F_i - \frac{1}{2!}\alpha_{ij} F_i F_j - \frac{1}{3!}\beta_{ijk} F_i F_j F_k - \frac{1}{4!}\beta_{ijkl} F_i F_j F_k F_l - \cdots \quad (1)$$

In such equation, α is the dipolar polarizability, β and γ are the first and second hyperpolarizabilities, while F is the applied electric field.

The dipolar polarizability is a tensor (3 × 3) with nine components that can be combined to give the isotropic contribution

$$\langle\alpha\rangle = \frac{1}{3}(\alpha_{xx} + \alpha_{yy} + \alpha_{zz}). \quad (2)$$

The isotropic polarizability can be used to infer the refractive index (n) using the Lorentz–Lorenz equation

$$\frac{n^2-1}{n^2+2} = \frac{4\pi\langle\alpha\rangle}{3V_{\text{mol}}}, \tag{3}$$

where V_{mol} is the molecular volume.

On the other hand, β is a cubic (3 × 3 × 3) tensor with twenty-seven components. However, the Kleinman symmetry rules [30] allow reducing this number to only ten distinct elements, which can be manipulated to give the static first-hyperpolarizability

$$\beta_{\text{total}} = \sqrt{\beta_x^2+\beta_y^2+\beta_z^2}, \tag{4}$$

where each component β_i is given as

$$\beta_i = \beta_{iii} + \frac{1}{3}\sum_j (\beta_{ijj}+\beta_{jij}+\beta_{jji}). \tag{5}$$

In the presence of frequency-dependent light, this quantity is better described by the hyper-Rayleigh scattering apparatus (β_{HRS}) [15] as

$$\beta_{\text{HRS}}(-2\omega;\omega,\omega) = \beta_{\text{HRS}} = \sqrt{\langle\beta_{ZZZ}^2\rangle + \langle\beta_{ZXX}^2\rangle}. \tag{6}$$

In such an equation,

$$\begin{aligned}\langle\beta_{ZZZ}^2\rangle = {} & \frac{1}{7}\sum_i^{x,y,z}\beta_{iii}^2 + \frac{1}{35}\sum_{i\neq j}^{x,y,z}\left(\beta_{iij}^2+4\beta_{jii}^2\right)\\ & + \frac{2}{35}\sum_{i\neq j}^{x,y,z}\left(\beta_{iii}\beta_{ijj}+4\beta_{jii}\beta_{iij}+4\beta_{iii}\beta_{jji}\right)\\ & + \frac{1}{105}\sum_{i\neq j\neq k}^{x,y,z}\left(\beta_{iij}\beta_{jkk}+\beta_{iij}\beta_{jkk}+\beta_{ijk}\beta_{jik}\right)\\ & + \frac{4}{105}\sum_{i\neq j\neq k}^{x,y,z}\left(\beta_{jii}\beta_{jkk}+2\beta_{ijk}^2\right)\end{aligned} \tag{7}$$

and

$$\begin{aligned}\langle\beta_{ZXX}^2\rangle = {} & \frac{1}{35}\sum_i^{x,y,z}\beta_{iii}^2 + \frac{4}{105}\sum_{i\neq j}^{x,y,z}\left(\beta_{iii}\beta_{ijj}+2\beta_{iij}^2\right)\\ & + \frac{1}{35}\sum_{i\neq j}^{x,y,z}\left(3\beta_{ijj}^2-2\beta_{iii}\beta_{jji}-2\beta_{iij}\beta_{jii}\right)\\ & - \frac{2}{105}\sum_{i\neq j\neq k}^{x,y,z}\left(\beta_{iik}\beta_{jjk}+\beta_{iij}\beta_{jkk}+\beta_{ijk}\beta_{jik}\right)\\ & + \frac{1}{105}\sum_{i\neq j\neq k}^{x,y,z}\left(2\beta_{ijk}^2+\beta_{ijj}\beta_{jkk}\right)\end{aligned} \tag{8}$$

Finally, $\langle\beta_{ZZZ}^2\rangle$ and $\langle\beta_{ZXX}^2\rangle$ give the polarization ratio

$$DR_{\text{HRS}} = \frac{\langle\beta_{ZZZ}^2\rangle}{\langle\beta_{ZXX}^2\rangle}. \tag{9}$$

The second hyperpolarizability (γ) is a fourth-rank tensor (3×3×3×3) with 81 components. For the all static case, it is possible to use again the Kleinman rules and work only with six components. Thus, the average second hyperpolarizability is given as [15]

$$\langle\gamma\rangle = \frac{1}{5}\left[\gamma_{xxxx}+\gamma_{yyyy}+\gamma_{zzzz}+2\left(\gamma_{xxyy}+\gamma_{xxzz}+\gamma_{yyzz}\right)\right] \tag{10}$$

On the other side, for nonzero frequencies, the Kleinman symmetry cannot be applied, and a free permutation of the indexes is not allowed. However, within the Electric-Field-Induced Second-Harmonic Generation setup, the middle indexes can be interchanged $\gamma_{ijkl} = \gamma_{ikjl}$. Such simplification allows us to work with only 15 components, and the third harmonic generation $\gamma(-3\omega;\omega,\omega,0) = \langle\gamma\rangle^{\text{THG}}$ is given as [15]

$$\langle\gamma\rangle^{\text{THG}} = \frac{1}{5}\left[\gamma_{xxxx}+\gamma_{yyyy}+\gamma_{zzzz}+2\left(\gamma_{xxyy}+\gamma_{xxzz}+\gamma_{yyzz}\right)\right] \tag{11}$$

Finally, all MC simulations and electronic structure calculations were carried out using respectively the DICE [31] and Gaussian 09 [32] packages. However, the entire NLO analysis was carried out using the Multiwfn code [33].

Table 1
The quantum mechanical and CHELPG values calculated for the molecular dipole moment using the CAM-B3LYP/6-311++G(*d,p*) level of theory and different environments:

	Ground State		Excited State	
Environment	QM	CHELPG	QM	CHELPG
Vacuum	4.34	4.44	5.33	5.27
C-PCM	4.89	4.98	6.29	6.24
ASEC	5.16	5.24	6.68	6.70

3. Results

3.1. Dipole moment and solute polarization

Maybe the most relevant environmental effect is the solute polarization mediated by the solvent molecules which can affect structural properties like nuclear magnetic parameters [28], vibrational frequencies [29,34], and a variety of optical processes [8,27]. Table 1 allows analyzing these effects for molecular dipole moment in the ground (μ_g) and first excited (μ_e) states. The results are calculated considering the electrostatic solvent models C-PCM and ASEC using the CAM-B3LYP/6-311++G(*d,p*) level of quantum mechanics. As can be seen, the quantum mechanical value of the dipole moment and its electrostatic adjustment (CHELPG) are very close for all situations. Thus, we shall keep the discussion on the CHELPG values, which were implemented in the classical MC simulations.

For several polar molecules like formamide [35] and uracil [36,37], the polarization due to solvent can increase the molecular dipole moment over 60% of the vacuum value. However, the NPE molecule is less susceptible to these effects. For the isolated molecule in a vacuum, the CHELPG scheme predicts a ground state dipole moment of 4.44 D. However, when the system is embedded in an aqueous environment, μ_g increases to 4.94 D, according to the C-PCM estimative. This means a weak polarization effect of almost 12.26% regarding the vacuum. On the other hand, the iterative procedure and the ASEC indicate a greater effect of 18%, which increases the ground state dipole moment to 5.25 D.

On the other side, the first excited state is more sensible to polarization due to solvent. For instance, at vacuum conditions, the CAM-B3LYP result indicates a dipole moment of 5.27 D. However, when the system is immersed in an aqueous environment, C-PCM and ASEC predict respectively 6.24 and 6.70 D, which means a polarization effect between 18 and 27%, concerning the gas-phase value.

3.2. Solute–solvent hydrogen bonds and the liquid structure

Since the excited and ground state geometries can differ structurally, different polarizations can be obtained in solution and, consequently, different solvent organizations around the solute molecule. For instance, the hydrogen bond formation is often affected in such cases, leading to significant changes in optical properties of solute in solution [8,10,38].

An understanding of the liquid structure can be performed by analyzing the minimal distance distribution function (MDDF) shown in Fig. 2. This function gives a spherical perspective of the salvation shell and shows how the solvent molecules are organized around the solute [39]. For both structures, there is a small shoulder at ~ 2 ∀, related to water molecules in the micro-solvation shell likely forming HB with the solute in its ground and first excited states. Integration of this shoulder up to 2 Å encloses 1.7 and 1.9 water molecules around the GS and ES structures, respectively. This result shows that the NPE molecule in GS and ES contains low hydration in the micro-solvation shell compared to other solutes studied before [26,27,40,41]. The first peak that comprehends the limits between 2.0 and 4.0 Å defines the first solvation shell, whereas the second peak between 4.0 and

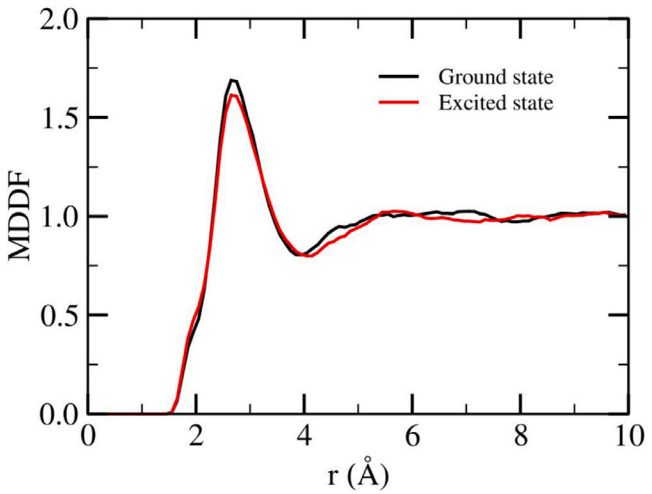

Fig. 2. Minimum distance distribution function (MDDF) for the NPE in the ground and first excited state in aqueous solution.

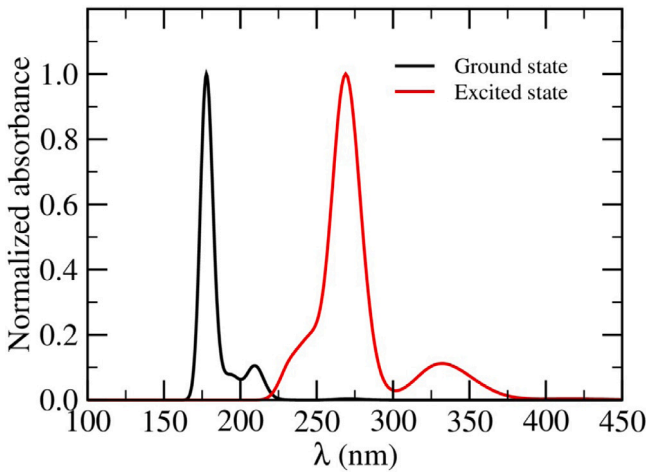

Fig. 3. The convolution of the ground (black line) and emission (red line) spectra of NPE molecule at vacuum conditions. The electronic excitations were obtained at the CAM-B3LYP/6-311++G(*d,p*) level of quantum mechanics.

Table 2
Structural information was obtained from RDF (radial distribution function) and HB (hydrogen bond) analysis to the NPE in the ground state (GS) and excited state (ES) both in water.

	Water molecules	
	GS	ES
Micro-solvation shell (up to 2.0 Å)	1.7	1.9
First shell (up to 4.0 Å)	40	40
Second shell (up to 7.5 Å)	161	158
HB average properties		
$\langle N_{HB}\rangle_N$ (nitrogen atom)	0.04	0.03
$\langle N_{HB}\rangle_O$ (oxygen atom)	1.04	1.16
$\langle N_{HB}\rangle_C$ (carbon atom)	0.05	0.04
$\langle N_{HB}\rangle_{total} = \langle N_{HB}\rangle_N + \langle N_{HB}\rangle_O + \langle N_{HB}\rangle_C$	1.15	1.23
$\langle R_{N\text{-}Ow}\rangle$ (Å)	3.18	3.20
$\langle R_{O\text{-}Ow}\rangle$ (Å)	2.89	2.90
$\langle R_{C\text{-}Ow}\rangle$ (Å)	3.14	3.14
$\langle E_{N\text{-}Ow}\rangle$ (cal/mol)	−2.15	−3.13
$\langle E_{O\text{-}Ow}\rangle$ (cal/mol)	−3.33	−3.73
$\langle E_{C\text{-}Ow}\rangle$ (cal/mol)	−1.43	−1.46

7.5 Å defines the second solvation shell. The integration of this first peak up to 4.0 Å gives the same number of water molecules (40), whereas the second peak up to 7.5 gives 161 and 158 water molecules around GS and ES structures, respectively. The statistics data obtained from the MDDF function for the NPE in both GS and ES are given in Table 2. Interestingly, it is noted that the number of water molecules around both NPE structures are very similar, but with the largest number of water molecules around the ES structure. From the QM point of view, it is expected that the number of water molecules in solvation shells to be similar for both ground and excited states, given the slight difference between its dipole moments.

The H-bonds between the NPE and water molecules were analyzed using the geometric and energetic criteria [42,43]. In our analysis, we consider that the NPE molecule has three types of H-bond acceptors: one nitrogen (N) atom, two oxygen (O) atoms, and six-carbon (C) atoms. These carbon atoms were considered H-bond acceptors because they are electron-rich atoms and participate in H-bonding as a π-bond with sp^2 and sp hybridization, donating electron density through the double bond [44,45]. In this work, we consider an H-bond formation when the distance between the acceptor (A) and donor (D) atoms, $R_{D-A} \leq 3.25$ ∀, and the angle between the vector defined by the acceptor–donor atoms and the vector defined by the hydrogen-donor bond, $\theta_{A\text{-}HD} \leq 40°$ and binding energy, $E_{ij} \leq -0.01$ kcal/mol.

After applying both criteria using the ORDER tool provided in DICE package [31], the average number of water molecules H-bonded to the oxygen atoms of GS and ES structures is 1.04 and 1.16 with a binding energy of −3.33 and −3.73 kcal/mol, respectively. For the nitrogen and carbon atoms, the average number of water molecules are very small, and similar value in these cases (0,04), but with different binding energy. In the case of the nitrogen atom, this energy is −2.15 kcal/mol for the GS and −3.13 kcal/mol for the ES, whereas, for the carbon atoms are −1.4 and −1.5 kcal/mol for the GS and ES structures, respectively. The results are presented in Table 1. The values of the H-bond number and energy in the carbon atoms are expected considering that from the energetic point of view, these carbon atoms form hydrogen bonds so much more weakly than nitrogen and oxygen atoms. In general, an average number of 1.15 and 1.23 water molecules H-bonded with an average energy of −3.5 and −4.2 kcal/mol was obtained to the GS and ES structures, respectively. This slight difference in H-bond number and energy, which also is reflected in the structural data, can be attributed to π-electron delocalization in the ring group, which tends to better stabilize the ES compared to the GS structure. Figure S1 shows the superposition of 600 MC configurations with water molecules H-bonded to the GS and ES structures.

3.3. Electronic excitations and Stokes shifts

Now we shall discuss the solvent effects on the electronic transitions in the NPE molecule. The NPE chromophore presents a benzene ring and an ethylene bond which are both hydrophobic groups. Therefore, long-range interactions and van der Waals forces are relevant for the photophysics description. For such a situation, the CAM-B3LYP DFT method has given a reliable description [29]. Thus, Table 3 shows the lowest-lying electronic absorption and emission considering different environment models and the CAM-B3LYP/6-311++G(*d,p*).

Fig. 3 shows the convoluted absorption spectrum (black line) obtained for NPE molecule in vacuum. Clearly, from this picture, it is possible to observe an intense excitation in the lowest-lying region of the spectrum. An analysis of the molecular orbitals involved in this excitation indicates an $n \rightarrow \pi^*$ symmetry (see Fig. 4) and occurs mainly on the ringside group, at 270.44 nm with an oscillator force of 0.0021. In an aqueous environment, according to electrostatic models, this excitation suffers a small hypsochromic shift. For instance, the C-PCM and ASEC methods indicate aspirations at 268.06 and 268.84 nm, respectively. Besides, the presence of the solvent increases the intensity of the transition to 0.0034 or 0.0042, depending on the solvent model used.

Table 3
The lowest-lying absorption ($n \rightarrow \pi^*$) and emission ($n \leftarrow \pi^*$) excitation were calculated using the CAM-B3LYP/6-311++G(*d,p*) for different environments and the corresponding Stokes shift:

Environment	$\pi \rightarrow \pi^*$ (nm)	f	$\pi \leftarrow \pi^*$ (nm)	f	Stokes (nm)
Gas-phase	270.44	0.0021	346.33	0.0047	75.89
C-PCM	268.06	0.0034	333.33	0.0313	65.27
ASEC	268.84	0.0042	332.08	0.0525	63.24
HB+PC	273.87 ± 0.43	0.0077 ± 0.0004	337.78 ± 0.92	0.0065 ± 0.0002	63.91 ± 1.35

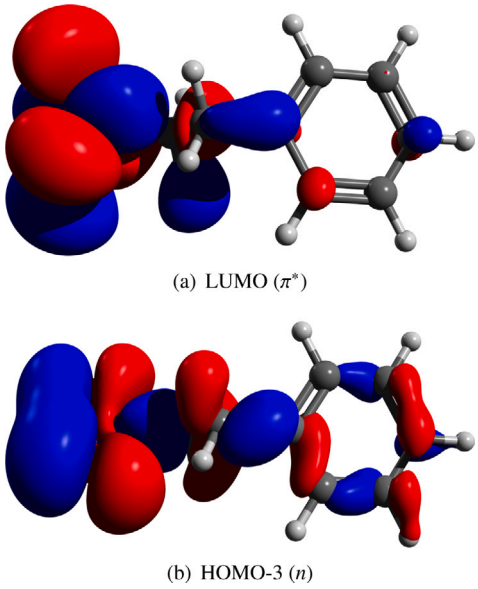

(a) LUMO (π^*)

(b) HOMO-3 (n)

Fig. 4. The Kohn–Sham molecular orbitals involved in the lowest-lying $n-\pi^*$ excitation obtained with CAM-B3LYP/6-311++G(*d,p*) level of quantum mechanics for the ground state in vacuum.

Table 4
The static dipole polarizability components (α) and refractive index n, components (β_x, β_y, and β_z) of the static first hyperpolarizability (β_{total}), the frequency-dependent (ω = 1059.61 nm) term (β_{HRS}), depolarization ratio (DR), the static and frequency-dependent second hyperpolarizabilities, $\langle\gamma\rangle$ and $\langle\gamma\rangle^{\text{THG}}$. All values were calculated using the CAM-B3LYP/6-311++G(*d,p*) quantum mechanical model:

Property	Gas-phase	C-PCM	ASEC
α_{xx}	21.12	23.08	20.49
α_{yy}	16.33	22.56	21.25
α_{zz}	11.80	12.71	3.01
$\langle\alpha\rangle$	15.66	20.90	15.58
V_{mol}	1543.38	1384.41	1171.39
n	1.49	1.80	1.68
E_{gap}	7.91	7.48	7.21
β_{total}	0.62	0.14	0.46
β_{HRS}	0.37	0.52	0.61
DR	2.28	1.52	2.10
$\langle\gamma\rangle$	11.06	25.91	10.83
$\langle\gamma\rangle^{\text{THG}}$	13.39	21.89	13.57

Units: E_{gap}/eV, $\alpha/10^{-24}$ esu, $\beta/10^{-30}$ esu, $\gamma/10^{-36}$ esu, and V_{mol}/a.u.
The conversion units are: α (1 a.u. = 1.4819 $\times 10^{-25}$) esu, β (1 a.u. = 8.63922 $\times 10^{-33}$ esu), γ (1 a.u. = 5.03670 $\times 10^{-40}$ esu).

However, the HB+PC solvation model gives other interpretations of the solvatochromism of NPE. Figure S2 shows the average of over one hundred MC configurations composed by the solute–solvent hydrogen-bonded structures embedded in the electrostatic field of the remaining three hundred water molecules accounted as point charges. According to this description, the lowest $n \rightarrow \pi^*$ should occur at 273.87 ± 0.43 nm with an oscillator force of 0.0077. Thus, what actually occurs is a bathochromic effect in relation to the molecule in a vacuum.

The HB+PC model goes beyond electrostatic models and includes explicitly solute–solvent hydrogen-bond structures. Consequently, it allows extending the wave function on the solvent molecules, which gives a better description of the phenomena. The disagreement between HB+PC and electrostatic models indicate that the explicit inclusion of solvent molecules is fundamental to understanding the solvatochromism of NPE.

Concerning the excited state energies, Fig. 3 also plots the emission spectra (red line) obtained for the NPE molecule at vacuum. Our TD-DFT analysis performed at gaseous conditions indicates that the lowest $n \leftarrow \pi^*$ is shifted 346.33 nm with an oscillator strength of 0.0047. After including the solvent contributions by the C-PCM and ASEC electrostatic model, the emissions at 333.33 and 332.08 nm are obtained, respectively, which means moderate blue shifts of 13 and 14.25 nm. On the other side, the inclusion of explicit solute–solvent interaction using the HB+PC model indicates an average value of 337.78 ± 0.92 nm, which is in good agreement with the electrostatic models. Furthermore, at least for the electronic excitations of NPE molecule, simple electrostatic models are enough to obtain a reliable understanding of the molecular photophysics.

As mentioned in the introduction, organics chromophores with strong Stokes shifts ($\Delta\lambda$ > 30 nm) are interesting for a variety of linear and nonlinear optical applications like solar cells, sensors, and biological probes against human diseases [6,7]. For the molecule in the gas phase, a displacement of 75.89 nm is obtained. However, in an aqueous environment, this Stokes shift decreases smoothly, assuming the values of 65.27 and 63.24 nm, according to the C-PCM and ASEC solvations models. Finally, the HB+PC analysis follows the same trend indicated by the electrostatic models and confirms a pronounced Stokes shift of 63.91 ± 1.35 nm.

3.4. Nonlinear optical properties

Dipolar polarizability

Table 4 shows the results for the dipole polarizability, $\langle\alpha\rangle$, calculated at vacuum and solvent using the CAM-B3LYP/6-311++G(*d,p*) level of quantum mechanics, besides the C-PCM and ASEC solvation models simulating the water solvent. For the isolated MPE molecule, the results indicate the dipole polarizability of 21.12×10^{-24} esu. Concerning the solvent contributions, there is a discrepancy between the C-PCM and ASEC models. The first of then indicates a polarization effect over 30%, increasing $\langle\alpha\rangle$ to 23.08×10^{-24} esu. On the other hand, the ASEC suggests that the contribution of the solvent is not significant for the dipole polarizability, indicating an average value of 20.49×10^{-24} esu.

The values obtained are considered superior to those reported for urea, which is a standard NLO chromophore. For instance, while Adant and co-workers have reported dipole polarizability of 5.40×10^{-24} esu using second and fourth-order of Moller–Plesset perturbation theory [46], Pluta used coupled-cluster with single, double, and perturbative triple excitations to report the value of 5.34×10^{-24} esu [47].

However, in comparison with other dyes designed especially for NLO uses, the title compound presents lower dipole polarizability values. For instance, Raiol and collaborators have estimated values for the varying from 50.86×10^{-24} to 77.23×10^{-24} esu, depending on the *cis–trans* isomerization [26]. Unfortunately, according to the Lorentz–Lorenz equation, great dipole polarizabilities can generate bigger refractive indexes. For instance, the above-mentioned dyes present a refractive index varying from 1.758 to 2.374 [26]. In a water environment, the

MPE molecule presents a lower refractive index. According to the C-PCM calculations $n = 1.80$. However, the ASEC results indicate a value of $n = 1.68$. Thus, this chromophore can be useful in optical fibers and sensors preparation.

First hyperpolarizability and the second harmonic generation

Table 4 shows the results for the parameters related to the second-harmonic generation calculated for gas-phase and different solvation models. Concerning the static hyperpolarizability at vacuum conditions, the CAM-B3LYP DFT indicates a value of 0.62×10^{-30} esu for β_{total}.

Concerning the solvent effects, analyzing the HOMO-LUMO energy-gap (E_{gap}), from gas-phase ($E_{\text{gap}} = 7.91$ eV) to solvent, both PCM and ASEC models indicate that the system becomes more like a semiconductor when in an aqueous environment. In fact, the results indicate values of 7.48 and 7.21 eV respectively for PCM and ASEC. According to Oldar and Chemla equation [48], in such a situation, the optical response should increase. However, both solvation models predict optical response lower than that obtained for the isolated molecule. The β_{total} the values are 0.14×10^{-30} and 0.46×10^{-30} esu, for PCM and ASEC respectively.

However, the inclusion of the frequency of light solves the problem mentioned above. For instance, the hyper-Rayleigh scattering technique indicates an in vacuum frequency-dependent hyperpolarizability (β_{HRS}) of 0.37×10^{-30} esu. In a solvent media, C-PCM indicates a value of 0.52×10^{-30} esu, while the ASEC suggests a 0.61×10^{-30} esu. Thus, the solvent improves between 24 and 26% of the NLO behavior of the chromophore. The values obtained for MPE are in good competition with other materials, like the urea molecule, which presents the first hyperpolarizability around 0.37×10^{-30} esu [49]. However, once NLO parameters are additive properties [50], molecular systems like urea and NPE, under their crystallized forms can be used for diverse NLO applications.

Second hyperpolarizability and the third harmonic generation

Concerning the third harmonic generation, the second hyperpolarizability (γ) is the most relevant parameter. Table 4 presents the results considering two situations. First, the low frequency or static case, in which the NLO parameter is written as a simple average $\langle\gamma\rangle$ mentioned above. However, for the frequency-dependent situation $\gamma(-3\omega;\omega,\omega,0)$, the second hyperpolarizability, is usually written similarly as the $\langle\gamma\rangle^{\text{THG}}$ also discussed above. Starting from the simplest case, the static form at vacuum conditions, the CAM-B3LYP DFT calculations indicate a value of 13.39×10^{-36} esu.

Concerning the solvent contribution, the continuum, and discrete solvation models, C-PCM and ASEC, show some discrepancies. For instance, the C-PCM calculations indicate a solvent effect that increases the second hyperpolarizability by 134.27% concerning the gas-phase value, indicating the value of 25.91×10^{-36} esu. However, the ASEC model indicates an almost imperceptible solvent contribution with $\langle\gamma\rangle = 10.83 \times 10^{-36}$ esu.

The inclusion of the frequency of light leads to similar observations. For instance, for the gaseous conditions, $\langle\gamma\rangle^{\text{THG}}$ is 13.39×10^{-36} esu, which is quite close to the static value. This finding indicates that high-power light improves moderately the THG effect. Concerning again the solvent contribution, the C-PCM calculations indicate a value of 21.89×10^{-36} esu, meaning great variation, ca. 63% with relation to vacuum.

Concerning other NLO materials, the NPE molecule presents an interesting THG behavior. For instance, Adant and collaborators have reported static values of 0.39×10^{-36} and 0.45×10^{-36} esu for the second hyperpolarizability [46]. In other words, the MPE molecule presents values almost one hundred times major than that found for urea, which is well stabilized NLO chromophore.

4. Conclusions

For the first time, it has been performed a systematic discussion on the linear and nonlinear optical properties of the 1-nitro-2-phenylethane molecule, which is the active principle found in the extract of *Aniba canelilla*, an Amazonian medicinal plant. This work pays special attention to the solvent contributions, which are carried by continuum and a sequential Monte Carlo/Quantum Mechanics procedure.

The analysis of the NLO properties is carried out considering the low frequency and frequency-dependent domain. The title molecule presents a lower refractive index and concerning the second and in particular the third harmonic generation the material presents promissory use in NLO. The electronic absorption and emission spectra also were characterized. The lowest-lying region of the spectra presents a strong $n-\pi^*$ excitation which suffers a strong Stokes shift in an aqueous environment. Consequently, the studied chromophore can be useful as a molecular probe or even in solar cells applications.

CRediT authorship contribution statement

Franco F. Almeida: Software, Investigation, Data curation. **Lucas Modesto-Costa:** Software, Investigation, Data curation, Graphical abstract, Writing – review. **Antonio R. da Cunha:** Software, Investigation, Data curation. **Darlisson A. Santos:** Investigation, Methodology, Writing. **Tarciso Andrade-Filho:** Investigation, Methodology, Writing. **Rodrigo Gester:** Conceptualization, Methodology, Investigation, Writing – review & editing, Supervision.

Declaration of competing interest

The authors declare that they have no known competing financial interests or personal relationships that could have appeared to influence the work reported in this paper.

Data availability

Data will be made available on request.

Acknowledgments

This study is financed in part by the Coordenação de Aperfeiçoamento de Pessoal de Nível Superior - Brasil (CAPES), Conselho Nacional de Desenvolvimento Científico e Tecnologico (CNPq), and Fundação de Amazônica de Amparo a Estudos e Pesquisas (FAPESPA).

Appendix A. Supplementary data

Supplementary material related to this article can be found online at https://doi.org/10.1016/j.cplett.2022.139867.

References

[1] A.B. de Lima, M.B. Santana, A.S. Cardoso, J.K.R. da Silva, J.G.S. Maia, J.C.T. Carvalho, P.J.C. Sousa, Antinociceptive activity of 1-nitro-2-phenylethane, the main component of Aniba canelilla essential oil, Phytomedicine 16 (2009) 555–559, http://dx.doi.org/10.1016/j.phymed.2008.10.007.

[2] J.L. Giongo, R.A. Vaucher, A.S.D. Silva, C.B. Oliveira, C.B. de Mattos, M.D. Baldissera, M.R. Sagrillo, S.G. Monteiro, D.L. Custódio, M.S. de Matos, P.T. Sampaio, H.F. Teixeira, L.S. Koester, V.F. da Veiga Junior, Trypanocidal activity of the compounds present in Aniba canelilla oil against Trypanosoma evansi and its effects on viability of lymphocytes, Microb. Pathogen. 103 (2017) 13–18, http://dx.doi.org/10.1016/j.micpath.2016.12.006.

[3] D.P. Souza, R.B. Pimentel, A.S. Santos, P.M. Albuquerque, A.V. Fernandes, S.D. Junior, J.T. Oliveira, M.V. Ramos, B. Rathinasabapathi, J.F. Gonçalves, Fungicidal properties and insights on the mechanisms of the action of volatile oils from Amazonian Aniba trees, Ind. Crops Prod. 143 (2020) 111914, http://dx.doi.org/10.1016/j.indcrop.2019.111914.

[4] R.J.B. de Siqueira, F.I.B. Macedo, L. de Fátima Leal Interaminense, G.P. Duarte, P.J.C. Magalhães, T.S. Brito, J.K.R. da Silva, J.G.S. Maia, P.J. da Cunha Sousa, J.H. Leal-Cardoso, S. Lahlou, 1-nitro-2-phenylethane, the main constituent of the essential oil of aniba canelilla, elicits a vago-vagal bradycardiac and depressor reflex in normotensive rats, Euro. J. Pharmacol. 638 (2010) 90–98, http://dx.doi.org/10.1016/j.ejphar.2010.03.060.

[5] L. Arruda-Barbosa, K.M.S. Rodrigues, F. das Chagas Vasconcelos Souza-Neto, G.P. Duarte, R.S. Borges, P.J.C. Magalhães, S. Lahlou, Vasorelaxant effects of 1-nitro-2-phenylethene in rat isolated aortic rings, Vascul. Pharmacol. 63 (2014) 55–62, http://dx.doi.org/10.1016/j.vph.2014.08.002.

[6] K. Huang, X. Jiao, C. Liu, Q. Wang, X. Qiu, S. He, L. Zhao, X. Zeng, Synthesis of a novel π-extended hybrid rhodamine dye with far-red fluorescence emission and its application in bioimaging, Dye. Pigment. 145 (2017) 561–569, http://dx.doi.org/10.1016/j.dyepig.2017.06.047.

[7] Z. Gao, Y. Hao, M. Zheng, Y. Chen, A fluorescent dye with large Stokes shift and high stability: synthesis and application to live cell imaging, RSC Adv. 7 (2017) 7604–7609, http://dx.doi.org/10.1039/C6RA27547H.

[8] V. Manzoni, R. Gester, A.R. da Cunha, T. Andrade-Filho, R. Gester, Solvent effects on Stokes shifts, and NLO response of thieno[3, 4-b]pyrazine: A comprehensive QM/MM investigation, J. Molecular Liquids 335 (2021) 115996, http://dx.doi.org/10.1016/j.molliq.2021.115996.

[9] A. Gonçalves, A. Raiol, A.R. da Cunha, V. Manzoni, T. Andrade-Filho, R. Gester, Insights on the crossing of the two lowest n-π^* and $\pi-\pi^*$ absorption lines of thieno[3,4-b]pyrazine in an aqueous environment, Chem. Phys. Lett. 768 (2021) 138366, http://dx.doi.org/10.1016/j.cplett.2021.138366.

[10] K. Coutinho, S. Canuto, Solvent effects in emission spectroscopy: A Monte Carlo quantum mechanics study of the $n \leftarrow \pi^*$ shift of formaldehyde in water, J. Chem. Phys. 113 (20) (2000) 9132–9139, http://dx.doi.org/10.1063/1.1320827.

[11] K. Coutinho, S. Canuto, The sequential Monte Carlo-quantum mechanics methodology. Application to the solvent effects in the Stokes shift of acetone in water, J. Mol. Struct.: THEOCHEM 632 (2003) 235–246, http://dx.doi.org/10.1016/s0166-1280(03)00302-6.

[12] T. Schneider, Nonlinear Optics in Telecommunications, Springer Berlin Heidelberg, 2004, http://dx.doi.org/10.1007/978-3-662-08996-5.

[13] P. Hohenberg, W. Kohn, Inhomogeneous electron gas, Phys. Rev. 136 (1964) B864–B871, http://dx.doi.org/10.1103/PhysRev.136.B864.

[14] W. Kohn, L.J. Sham, Self-consistent equations including exchange and correlation effects, Phys. Rev. 140 (1965) A1133–A1138, http://dx.doi.org/10.1103/PhysRev.140.A1133.

[15] H.A. Kurtz, D.S. Dudis, Quantum mechanical methods for predicting nonlinear optical properties, in: Reviews in Computational Chemistry, John Wiley & Sons, Inc., 2007, pp. 241–279, http://dx.doi.org/10.1002/9780470125892.ch5.

[16] T. Yanai, D.P. Tew, N.C. Handy, A new hybrid exchange–correlation functional using the Coulomb-attenuating method (CAM-B3LYP), Chem. Phys. Lett. 393 (2004) 51–57, http://dx.doi.org/10.1016/j.cplett.2004.06.011.

[17] T. Clark, J. Chandrasekhar, G.W. Spitznagel, P.V. RaguŠSchleyer, Efficient diffuse function-augmented basis sets for anion calculations. III. The 3-21+G basis set for first-row elements, Li-F, J. Comput. Chem. 4 (1983) 294–301, http://dx.doi.org/10.1002/jcc.540040303.

[18] R. Krishnan, J.S. Binkley, R. Seeger, J.A. Pople, Self-consistent molecular orbital methods. XX. a basis set for correlated wave functions, J. Chem. Phys. 72 (1980) 650–654, http://dx.doi.org/10.1063/1.438955.

[19] V. Barone, M. Cossi, Quantum calculation of molecular energies and energy gradients in solution by a conductor solvent model, J. Phys. Chem. A 102 (1998) 1995–2001, http://dx.doi.org/10.1021/jp9716997.

[20] M. Cossi, N. Rega, G. Scalmani, V. Barone, Energies, structures, and electronic properties of molecules in solution with the C-PCM solvation model, J. Comput. Chem. 24 (2003) 669–681, http://dx.doi.org/10.1002/jcc.10189.

[21] W.L. Jorgensen, J. Chandrasekhar, J.D. Madura, R.W. Impey, M.L. Klein, Comparison of simple potential functions for simulating liquid water, J. Chem. Phys. 79 (2) (1983) 926–935, http://dx.doi.org/10.1063/1.445869.

[22] J. Pranata, S.G. Wierschke, W.L. Jorgensen, OPLS potential functions for nucleotide bases. Relative association constants of hydrogen-bonded base pairs in chloroform, J. Am. Chem. Soc. 113 (1991) 2810–2819, http://dx.doi.org/10.1021/ja00008a002.

[23] C.M. Breneman, K.B. Wiberg, Determining atom-centered monopoles from molecular electrostatic potentials. The need for high sampling density in formamide conformational analysis, J. Comput. Chem. 11 (1990) 361–373, http://dx.doi.org/10.1002/jcc.540110311.

[24] S. Miertuš, E. Scrocco, J. Tomasi, Electrostatic interaction of a solute with a continuum. a direct utilizaion of AB initio molecular potentials for the prevision of solvent effects, Chem. Phys. 55 (1981) 117–129, http://dx.doi.org/10.1016/0301-0104(81)85090-2.

[25] K. Coutinho, H. Georg, T. Fonseca, V. Ludwig, S. Canuto, An efficient statistically converged average configuration for solvent effects, Chem. Phys. Lett. 437 (2007) 148–152, http://dx.doi.org/10.1016/j.cplett.2007.02.012.

[26] A. Raiol, A.R. da Cunha, V. Manzoni, T. Andrade-Filho, R. Gester, Solvent enhancement and isomeric effects on the NLO properties of a photoinduced cis-trans azomethine chromophore: A sequential MC/QM study, J. Molecular Liquids (2021) 116887, http://dx.doi.org/10.1016/j.molliq.2021.116887.

[27] V. Manzoni, L. Modesto-Costa, J.D. Nero, T. Andrade-Filho, R. Gester, Strong enhancement of NLO response of methyl orange dyes through solvent effects: A sequential Monte Carlo/DFT investigation, Opt. Mater. 94 (2019) 152–159, http://dx.doi.org/10.1016/j.optmat.2019.05.018.

[28] R.M. Gester, H.C. Georg, S. Canuto, M.C. Caputo, P.F. Provasi, NMR chemical shielding and spin-spin coupling constants of liquid NH3: A systematic investigation using the sequential QM/MM method, J. Phys. Chem. A 113 (2009) 14936–14942, http://dx.doi.org/10.1021/jp9050484.

[29] M.V.A. Damasceno, V. Manzoni, L. Modesto-Costa, G.M. Moura, J.D. Nero, A. Torres, R. Gester, Solvent effects on low-lying absorptions and vibrational spectra of thieno[3, 4-b]pyrazines: the role of unconventional c–H···N bonds, Chem. Pap. 73 (2019) 1519–1527, http://dx.doi.org/10.1007/s11696-019-00703-2.

[30] D.A. Kleinman, Nonlinear dielectric polarization in optical media, Phys. Rev. 126 (1962) 1977–1979, http://dx.doi.org/10.1103/PhysRev.126.1977.

[31] H.M. Cezar, S. Canuto, K. Coutinho, DICE: A Monte Carlo code for molecular simulation including the configurational bias Monte Carlo method, J. Chem. Inf. Model. 60 (2020) 3472–3488, http://dx.doi.org/10.1021/acs.jcim.0c00077.

[32] M.J. Frisch, G.W. Trucks, H.B. Schlegel, G.E. Scuseria, M.A. Robb, J.R. Cheeseman, G. Scalmani, V. Barone, G.A. Petersson, H. Nakatsuji, X. Li, M. Caricato, A. Marenich, J. Bloino, B.G. Janesko, R. Gomperts, B. Mennucci, H.P. Hratchian, J.V. Ortiz, A.F. Izmaylov, J.L. Sonnenberg, D. Williams-Young, F. Ding, F. Lipparini, F. Egidi, J. Goings, B. Peng, A. Petrone, T. Henderson, D. Ranasinghe, V.G. Zakrzewski, J. Gao, N. Rega, G. Zheng, W. Liang, M. Hada, M. Ehara, K. Toyota, R. Fukuda, J. Hasegawa, M. Ishida, T. Nakajima, Y. Honda, O. Kitao, H. Nakai, T. Vreven, K. Throssell, J.A. Montgomery, J.E. Peralta Jr., F. Ogliaro, M. Bearpark, J.J. Heyd, E. Brothers, K.N. Kudin, V.N. Staroverov, T. Keith, R. Kobayashi, J. Normand, K. Raghavachari, A. Rendell, J.C. Burant, S.S. Iyengar, J. Tomasi, M. Cossi, J.M. Millam, M. Klene, C. Adamo, R. Cammi, J.W. Ochterski, R.L. Martin, K. Morokuma, O. Farkas, J.B. Foresman, D.J. Fox, Gaussian 09, Revision A.02, 2016, Gaussian Inc. Wallingford CT.

[33] T. Lu, F. Chen, Multiwfn: A multifunctional wavefunction analyzer, 33, (5) 2011, pp. 580–592, http://dx.doi.org/10.1002/jcc.22885.

[34] H.C. Georg, S. Canuto, Electronic properties of water in liquid environment. A sequential QM/MM study using the free energy gradient method, J. Phys. Chem. B 116 (36) (2012) 11247–11254, http://dx.doi.org/10.1021/jp304201b.

[35] R. Gester, M.V. Damasceno, S. Canuto, V. Manzoni, A theoretical study of the magnetic shielding of 15N of formamide in liquid water, J. Molecular Liquids 320 (2020) 114415, http://dx.doi.org/10.1016/j.molliq.2020.114415.

[36] R. Gester, R.S.G. Carrano, P.F. Provasi, C. Bistafa, S. Canuto, Theoretical analysis of the influence of CλH··· O bonds on the NMR constants of uracil in DMSO, Theor. Chem. Accounts 139 (10) (2020) http://dx.doi.org/10.1007/s00214-020-02670-4.

[37] R.M. Gester, C. Bistafa, H.C. Georg, K. Coutinho, S. Canuto, Theoretically describing the 17o magnetic shielding constant of biomolecular systems: uracil and 5-fluorouracil in water environment, Theor. Chem. Accounts 133 (2013) http://dx.doi.org/10.1007/s00214-013-1424-y.

[38] C. Reichardt, T. Welton, Solvents and Solvent Effects in Organic Chemistry, Wiley-VCH Verlag GmbH & Co. KGaA, 2010, http://dx.doi.org/10.1002/9783527632220.

[39] H.C. Georg, K. Coutinho, S. Canuto, Solvent effects on the UV-visible absorption spectrum of benzophenone in water: A combined Monte Carlo quantum mechanics study including solute polarization, J. Chem. Phys. 126 (3) (2007) 034507, http://dx.doi.org/10.1063/1.2426346.

[40] C. Bistafa, L. Modesto-Costa, S. Canuto, A complete basis set study of the lowest $n-\pi^*$ and $\pi-\pi^*$ electronic transitions of acrolein in explicit water environment, Theor. Chem. Accounts 135 (5) (2016) http://dx.doi.org/10.1007/s00214-016-1891-z.

[41] M.V.A. Damasceno, B.J.C. Cabral, K. Coutinho, Structure and electronic properties of hydrated mesityl oxide: a sequential quantum mechanics/molecular mechanics approach, Theor. Chem. Accounts 131 (5) (2012) http://dx.doi.org/10.1007/s00214-012-1214-y.

[42] M. Mezei, D.L. Beveridge, Theoretical studies of hydrogen bonding in liquid water and dilute aqueous solutions, J. Chem. Phys. 74 (1) (1981) 622–632, http://dx.doi.org/10.1063/1.440819.

[43] M.G. Sceats, S.A. Rice, The water–water pair potential near the hydrogen bonded equilibrium configuration, J. Chem. Phys. 72 (5) (1980) 3236–3247, http://dx.doi.org/10.1063/1.439560.

[44] O. Loveday, J. Echeverría, Methyl groups as hydrogen bond acceptors via their sp3 carbon atoms, Cryst. Growth Des. 21 (10) (2021) 5961–5966, http://dx.doi.org/10.1021/acs.cgd.1c00853.

[45] H. Suezawa, T. Yoshida, Y. Umezawa, S. Tsuboyama, M. Nishio, CH/π interactions implicated in the crystal structure of transition metal compounds - A database study, Eur. J. Inorg. Chem. 2002 (12) (2002) 3148–3155, http://dx.doi.org/10.1002/1099-0682(200212)2002:12<3148::aid-ejic3148>3.0.co;2-x.

[46] C. Adant, M. Dupuis, J.L. Bredas, Ab initio study of the nonlinear optical properties of urea: Electron correlation and dispersion effects, Int. J. Quantum Chem. 56 (S29) (1995) 497–507, http://dx.doi.org/10.1002/qua.560560853.

[47] T. Pluta, A.J. Sadlej, Electric properties of urea and thiourea, J. Chem. Phys. 114 (1) (2001) 136, http://dx.doi.org/10.1063/1.1328398.

[48] J.L. Oudar, D.S. Chemla, Hyperpolarizabilities of the nitroanilines and their relations to the excited state dipole moment, J. Chem. Phys. 66 (6) (1977) 2664–2668, http://dx.doi.org/10.1063/1.434213.

[49] M.J. Alam, A.U. Khan, M. Alam, S. Ahmad, Spectroscopic (FTIR, FT-Raman, 1H NMR and UV–Vis) and DFT/TD-DFT studies on cholesteno [4,6-b,c]-2′,5′-dihydro-1′,5′-benzothiazepine, J. Mol. Struct. 1178 (2019) 570–582, http://dx.doi.org/10.1016/j.molstruc.2018.10.063.

[50] K. Wu, J.G. Snijders, C. Lin, Reinvestigation of hydrogen bond effects on the polarizability and hyperpolarizability of urea molecular clusters, J. Phys. Chem. B 106 (35) (2002) 8954–8958, http://dx.doi.org/10.1021/jp014181i.